Title
In-Situ Fracture Stiffness Determination

Authors
Hesler, G.J.
Zheng, Z.
Myer, L.R.

Publication Date
1990

UC-820
LBL-28444

Lawrence Berkeley Laboratory
UNIVERSITY OF CALIFORNIA

EARTH SCIENCES DIVISION

To be presented at the 31st U.S.
Symposium on Rock Mechanics,
Golden, CO, June 18–20, 1990, and
to be published in the Proceedings

In-Situ Fracture Stiffness Determination

G.J. Hesler III, Z. Zheng, and L.R. Myer

January 1990

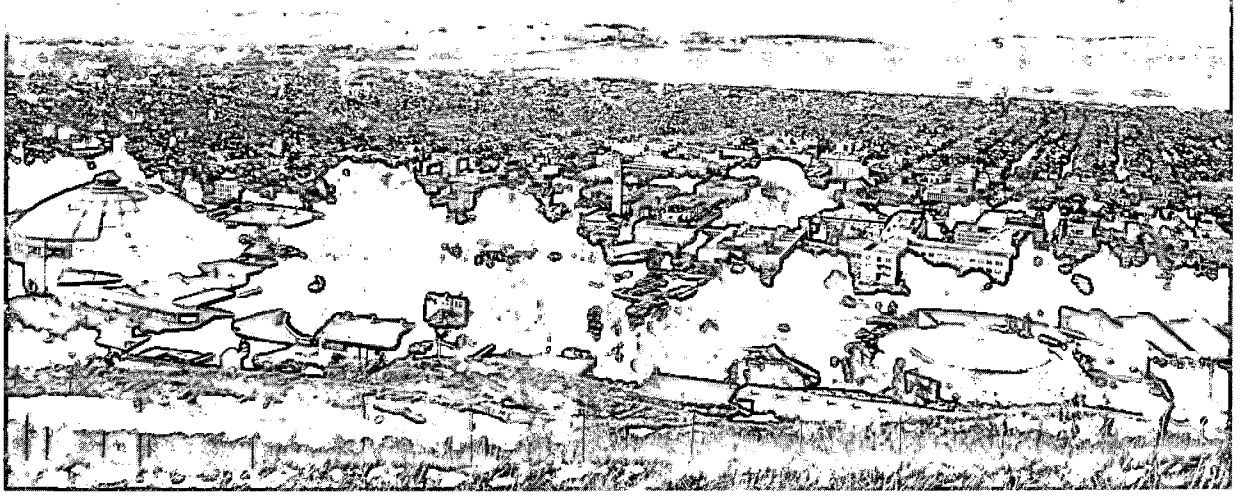

Prepared for the U.S. Department of Energy under Contract Number DE-AC03-76SF00098.

DISCLAIMER

LBL-28444

In-Situ Fracture Stiffness Determination

G. J. Hesler, III,[1] *Z. Zheng,*[2] *and L. R. Myer*[3]

[1]Department of Materials Science
and Mineral Engineering
University of California
Berkeley, California 94720

[2]Terra Tek, Incorporated
Salt Lake City, Utah 84108

[3]Earth Sciences Division
Lawrence Berkeley Laboratory
University of California
Berkeley, California 94720

January 1990

This work was supported by the Director, Office of Civilian Radioactive Waste Management, Office of Facilities Siting and Development, Siting and Facilities Technology Division, of the U.S. Department of Energy under Contract No. DE-AC03-76SF00098.

In-Situ fracture stiffness determination

G. J. HESLER, III
Department of Materials Science and Mineral Engineering,
University of California, Berkeley, California, USA

Z. ZHENG
Terra Tek, Incorporated,
Salt Lake City, Utah, USA

L. R. MYER
Earth Sciences Division, Lawrence Berkeley Laboratory,
University of California, Berkeley, California, USA

ABSTRACT: In-situ experiments to determine the hydrologic and mechanical characteristics of large naturally occurring fractures have been conducted at the NAGRA test site in Grimsel, Switzerland. In addition to seismic measurements across a fracture zone in the FRI test area and flow measurements into the zone, deformation of the fracture resulting from pressurization of the zone was also measured. The deformation is modeled in three different ways: as a mathematical crack employing linear elastic fracture mechanics; as a mathematical crack with an additional restraining stiffness between the faces of the crack, and as a row of coplanar two-dimensional cracks.

INTRODUCTION

In recent years with the increasing concern over the proper disposal of nuclear wastes, the modelling of potential nuclear waste disposal sites, and in particular of geologic discontinuities of these sites, has received increasing attention. The behavior of fractures and fracture zones as possible conduits for water into and out of repositories, and as locations for possible future deformation or failure needs to be accurately defined. Seismic methods have potential in providing a way to extrapolate from what is known from surface observations or borehole logging to what is present in the rock mass. Recent work (Pyrak-Nolte et al., 1987; Myer et al., 1990) has demonstrated on a laboratory scale that there are qualitative and quantitative relationships between seismic and hydrologic properties of fractured rock because of the dependence of both of these properties on the mechanical stiffness of the fractures. Theoretical and laboratory work (Schoenberg, 1980; Pyrak-Nolte, 1990) have shown that changes in seismic velocities and amplitudes can be related to the mechanical stiffness of individual fractures and joints in the rock. Transferring this knowledge to field applications is difficult in that little is known of the stiffness of fractures in-situ. To this end a fracture pressurization experiment was conducted at the Nagra Grimsel Test Site on a naturally occurring fracture zone. Measurements of pressure and deformation have been used to develop three models to describe the deformation behavior of the fracture.

DESCRIPTION OF THE EXPERIMENT

The fracture zone was intersected by two boreholes which were drilled between two tunnels. Results of previous hydrologic testing and inspection of cores showed that the principal fluid conductor consisted of a single, narrow fracture zone intersected by the boreholes. Hydraulic packers, incorporating sensitive displacement transducers to measure deformation (BOFEX) were installed in each borehole as shown in Figure 1. The distance between

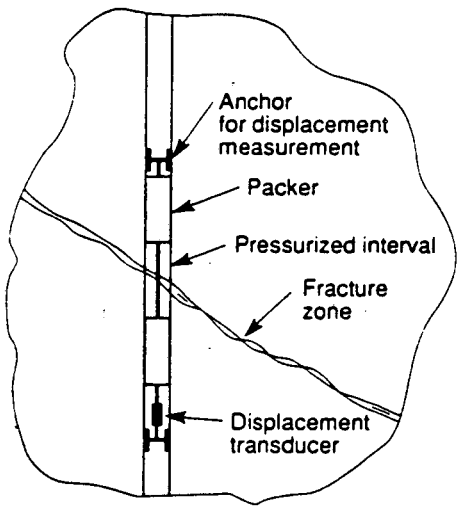

Figure 1. Plan view showing orientation of borehole 87.001 with the fault zone, and the location of hydraulic packers and transducers.

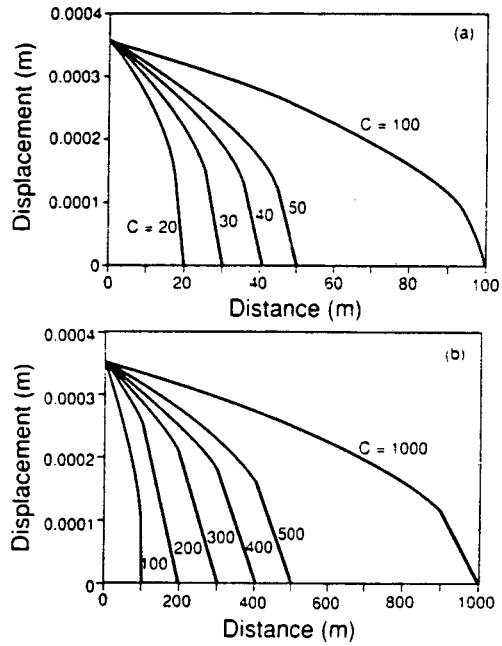

Figure 2. Displacements $\delta^{II}_{(o)}$ at the midpoint of a single crack assuming l = 13.6 m in Eq. (2).

anchors of the BOFEX was 1.5 m. The output of the displacement transducer was ± 10.0 V for a total possible displacement of ± 6.35 mm. With a 1 mV sensitivity provided by electronic instrumentation, the displacement resolution was 0.64 μm. The interval between the packers in one borehole was pressurized to 19 bars for a period of 17 hours. At the end of this period cumulative deformation experienced in the pressurized borehole was 2.2 x 10^{-6} m, while in the borehole, 10 meters away, the pressure had risen to 1.9 bars, but with no measurable displacement.

MODELLING OF THE RESULTS

In its simplest form the fracture can be modelled as two half-spaces separated by an interface in partial contact. Assuming a pressure of 19 bars and deformation of 1.42 x 10^{-6} m (corrected for the angle between the borehole and the plane of the fracture zone) the stiffness, κ, of the interface is given by:

$$\kappa = \frac{p}{\delta} = \frac{1.9 \times 10^{6}\ \text{Pa}}{1.42 \times 10^{-6}\ \text{m}} = 1.34 \times 10^{12}\ \text{Pa/m} \qquad (1)$$

where p is the pressure and δ is the fracture displacement. Implicitly assumed in this calculation is that the pressure was uniform across the face of the fracture. Since the pressure distribution was not uniform, and was of limited extent, Eq. (1) yields a conservative (high) estimate of the stiffness.

If it is assumed that the fracture can be modelled as a single fracture, or mathematical crack in plane strain subject to a non-uniform pressure distribution, linear elastic fracture mechanics can be used to find the displacements of the crack surfaces. The pressure distribution is approximated as a cubic polynominal of the form

$$P = P_o\,(a_o + a_1\,x + a_2\,x^2 + a_3\,x^3) \qquad (2)$$

with the constraints

$$P\big|_{x=0} = P_o = \text{constant} \quad P\big|_{x=l} = 0$$

$$\frac{dp}{dx}\Big|_{x=l} = 0 \quad \frac{d^2P}{dx^2}\Big|_{x=0} = 0$$

The coefficients a_i resulting from these constraints are:

$$a_o = 1\,, \quad a_1 = -\frac{3}{2l}, \quad a_2 = 0, \quad a_3 = \frac{1}{2l^3}$$

For a P_o = 19 bars at x = 0 , and P = 1.87 bars at x = 10.0 m, the value of l was calculated to be 13.6 m. To calculate displacements it is first necessary to obtain expressions for the model I stress intensity factor, K_I. For an elliptical crack of length 2c and point loads of magnitude P located at a distance x = b from the midpoint of the crack, K_I is given by:

$$K_I = \frac{2P\sqrt{c}}{\sqrt{\pi}} \cdot \frac{1}{\sqrt{c^2 - b^2}} \tag{3}$$

Integrating Eq. (3) for a pressure distribution yields the stress intensity factor for this configuration. Substituting Eq. (2) into (3) and performing the indicated integration yields

$$K_I = 2\sqrt{\frac{c}{\pi}}\, P_o \left\{ \sin^{-1}\left(\frac{l}{c}\right) + \frac{3}{2}\,\frac{c}{l}\sqrt{1 - \frac{l^2}{c^2}} - \frac{3c}{2l} + \right. \tag{4}$$

$$\left. + \frac{c^3}{2l^3}\left[-\sqrt{1 - \frac{l^2}{c^2}} + \frac{1}{3}\left(1 - \frac{l^2}{c^2}\right)^{3/2} + \frac{2}{3} \right] \right\}$$

With K_I known, the displacements normal to the plane of the crack can be given as a function of the position x from the midpoint of the crack:

$$\delta_{(x)} = \frac{2K_I}{E}\sqrt{\frac{2(c-x)}{\pi}}\,(1-\nu^2) \tag{5}$$

where ν is the Poisson's ratio of the material matrix. Displacements for the pressure distribution in Eq. (2) for a Young's modulus E of 42.7 GPa and a Poisson's ratio ν = 0.25 are plotted against distance from the center of the crack for different crack lengths in Figure 2. These plots show that for crack lengths greater than 20 m, there is no dependence of deformation at the center of the crack on crack length. More importantly, the plots shown that the calculated deformation at the center of the crack is two orders of magnitude higher than that measured in the field. The single pressurized crack model therefore does not model the physical reality of what was observed.

A more realistic model incorporates the notion that the surfaces of the crack are in partial contact. The single crack model was therefore modified to include an additional uniform stiffness between the faces of the crack, as shown in Figure 3(a). Assuming elastic deformation only, the problem of the pressurized crack with stiffness is solved by decomposition into two simpler problems and employing the principle of superposition. The two simpler problems involve: an elliptic crack subjected to the pressure distribution of Eq. (2), but

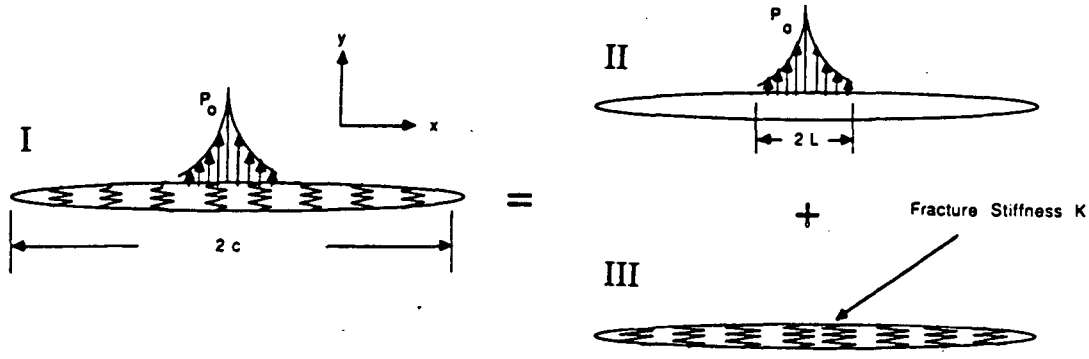

Figure 3. Modelling the injection experiment as a pressurized crack with stiffness. Assuming elasticity, Model I is decomposed into two single models II and III.

without any additional stiffness (Fig. 3b); and a geometrically identical crack with an additional uniform stiffness K (Fig. 3c).

By superposition the deformation of the composite crack (I) is related to that of the pressurized crack (II) and the crack with additional stiffness (III) by

$$\delta^{I}_{(x)} = \delta^{II}_{(x)} + \delta^{III}_{(x)} \tag{6}$$

where $\delta^{I}_{(x)}$ is the deformation at a distance x from the center of the crack for model I. $\delta^{I}_{(x)}$ is can be approximated from the measurements made in the field, while $\delta^{II}_{(x)}$ is calculable from Eq. (5). The difference between the measurements recorded in the field $\delta^{I}_{(x)}$, and $\delta^{II}_{(x)}$ represent the restraint due to the additional stiffness K and is given by

$$\delta^{III}_{(x)} = \delta^{I}_{(x)} - \delta^{II}_{(x)} \tag{7}$$

The additional pressure P'(x) which must be applied in III to yield these displacements is given by

$$P'(x) = \kappa \delta^{I}_{(x)} \tag{8}$$

As $\delta^{I}_{(x)}$ is not known for values other than x = 0 it is assumed that $\delta^{I}_{(x)}$ and $\delta^{II}_{(x)}$ differ only by a constant of proportionality given by $\delta^{I}_{(o)}/\delta^{II}_{(o)}$; where $\delta^{II}_{(x)}$ is calculated from Eq. (5). Then Eq. (8) becomes

$$P'(x) = \kappa \left[\frac{\delta^{I}_{(o)}}{\delta^{II}_{(o)}}\right] \delta^{II}_{(x)} \tag{9}$$

and Eq. (7) can be rewritten as

$$\delta^{III}_{(x)} = \delta^{I}_{(x)} - \delta^{II}_{(x)} = \left[\frac{\delta^{I}_{(o)}}{\delta^{II}_{(o)}} - 1\right] \delta^{II}_{(x)} \tag{10}$$

It is then possible to determine the mode I stress intensity factor for model III. Substituting the expression for P'(x) in Eq. (9) into Eq. (3), and integrating for K_I^{III}, this yields

$$K_I^{III} = 2\sqrt{\frac{c}{\pi}}\,\kappa \left[b_o \frac{\pi}{2} + b_1 c + b_2 c^2 \left(\frac{\pi}{4}\right) + \frac{2}{3} b_3 c^3\right] \frac{\delta^{I}_{(o)}}{\delta^{II}_{(o)}} \tag{11}$$

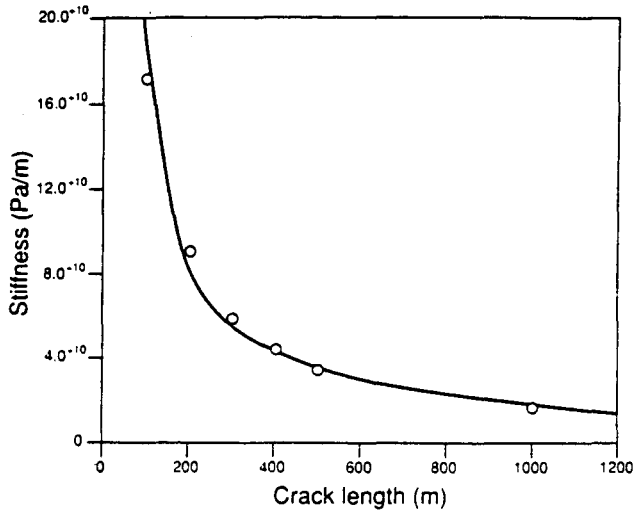

Figure 4. Predicted fracture stiffness as a function of crack length for the crack with additional stiffness.

where the coefficients b_i are from a third-order polynomial equation for deformation of the pressurized crack (II). Substituting the expression Eq. (11) for K_I^{III} into Eq. (5) gives

$$\delta^I_{(o)} - \delta^{II}_{(o)} = \frac{4c}{\pi} \frac{1-\nu^2}{E} \left\{ \kappa \frac{\delta^I_{(o)}}{\delta^{II}_{(o)}} \left[b_o \frac{\pi}{2} + b_1 c + b_2 c^3 \frac{\pi}{4} + \frac{2}{3} b_3 c^3 \right] \right\} \qquad (12)$$

For different values of crack length it is then possible to determine the corresponding stiffness. These are plotted in Figure 4. While the extent of the fractured zone is not known, it is expected to be in excess of ten times the pressurized region. For crack lengths of this order of magnitude Eq. (12) yields values of κ on the order of 4×10^{10} to 2×10^{11} Pa/m, or almost two orders of magnitude less than that derived for two half-spaces joined by a stiffness as in Eq. (1). Laboratory tests performed by Pyrak-Nolte et al., (1987) suggest that the values of stiffness of naturally occurring fractures in granite could be in the range of 10^{12} to 10^{13} Pa/m. Much lower in-situ values for the fracture zone in this study might have two causes: first, the fracture zone contained gouge, which would lower its stiffness; second, the field measurements were performed on a much larger scale. If void size is scale is invariant then stiffness should decrease roughly as the inverse square of sample size.

The third model developed is that of a row of a finite number of two-dimensional coplanar cracks of equal crack length, and uniform spacing of 2b. In this model the ligaments of material between the cracks can be taken to represent the areas of contact between the faces of the fracture, and the cracks to represent those areas not in contact.

Simulations of the model for different crack spacings 2b and ratios of crack length to crack spacing c/b were conducted assuming the material properties already noted above in the TWODD two-dimensional boundary element program developed by Crouch and Starfield (1983). Crack spacing, 2b, ranged from 50 m as upper limit to 0.10 m as the lower limit. Crack length to crack spacing ratios c/b ranged from 0.05 to 0.99. The range of c/b values for each b was selected to best match observed results. The deformations were calculated for a position of 0.75 m above the midpoint of the center fracture.

The number of cracks for each simulation was chosen to accommodate the extent of the pressure distribution as observed in the field so that the row of cracks extended from x = 0 m to x = ± 13.6 m with the first crack centered at the origin. The pressure distribution was

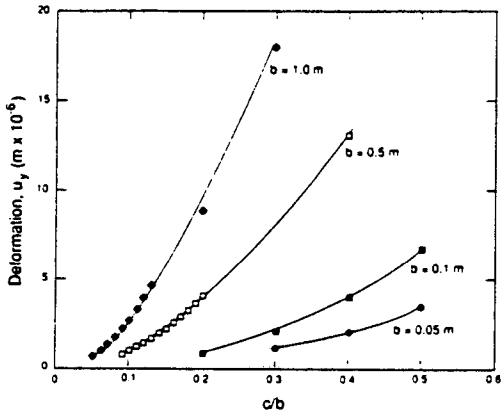

Figure 5. Deformation between two points located 0.75 m either side of the midpoint of the center crack of a row of pressurized coplanar cracks.

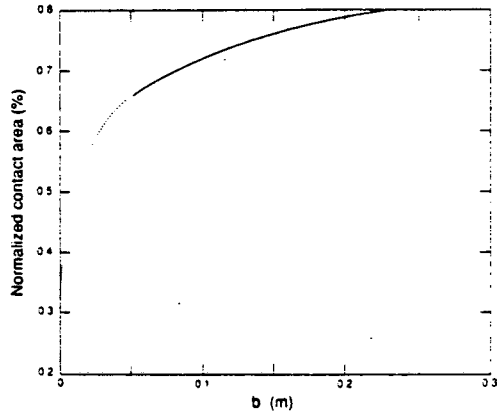

Figure 6. Normalized contact area of fracture faces as a function of crack half spacing b for a deformation of 1.42 x 10^{-6} m.

assumed to act only within the cracks. The effect of additional unpressurized cracks was found to be minimal. Simulations were run for a single crack of 40 m length containing the entire pressure distribution and c/b = 0.8. Additional deformation for fourteen cracks on either side of the pressurized crack increased the deformation by less than 6%. Simulations for a smaller crack spacing of 2b = 2 m and a c/b ranging from 0.95 to 0.99 showed an even less pronounced effect on the deformation.

Simulations were run for crack spacing values ranging from 2b = 0.1 m to 2b = 1.0 m, for a range of c/b values from 0.05 to 0.99. Results for the simulation are shown in Figure 5. All simulations show the same trend of deformation increasing exponentially with increasing c/b, or decreasing contact area. The effect of the crack spacing 2b on the deformation is significant; for a given c/b, the deformation increases exponentially with increasing b. Proportional decrease in c/b for a given deformation is less than the proportional increase in b. If Figure 5 is interpreted in terms of contact area, for a given contact area deformation increases with increasing b, and the contact area required to provide a given deformation increases with increasing b. This implies that the smaller the crack spacing, the smaller the ligaments between the cracks and therefore the contact areas have to be for a given deformation. This corroborates the work of Hopkins (1987), who found that for a given contact area, the smaller the individual areas of contact the higher the stiffness of a fracture.

The horizontal line in Figure 5 represents the measured deformation in situ (1.42 x 10^{-6} m). It is seen that for a given crack size quite large spacings are required to match the observed results. Figure 6 is a plot of the percent contact area (1 - c/b) required to match the observed information as a function of crack spacing. This shows that for spacing 2b of 0.1 m the contact area would still have to be about 66%. Because of limitations in computing capacity it was not possible to make calculations of deformation for b less than 0.05 m. An extrapolation of the curve in Figure 6 (dotted line), based on a curve fit of the values obtained at larger values of b shows that even if the crack spacing 2b were 0.05 m, the contact area would be about 59%.

An independent assessment of the contact area in the fracture zone could not be made. However, since the zone contained gouge material, high contact areas might be expected. Another possibility is that the fluid in the fracture was confined to channels and did not have access to all available void space.

CONCLUSIONS

Three models have been developed to model the deformation resulting from an in-situ pressurization test of a fracture zone. A single crack model based on linear elastic fracture mechanics proved to be too compliant, producing deformations two orders of magnitude more than those measured. A similar model also based on linear elastic fracture mechanics with an additional introduced stiffness between the faces of a single crack was developed, which yielded deformations on the scale measured in the field. Introducing an additional stiffness between crack faces is similar to accounting for the effect of areas of contact between fracture crack faces. This model is useful in that it allows a direct calculation for the fracture stiffness, which in turn can be used to determine the effect on a transmitted seismic wave. The third model, that of a row of a finite number of two-dimensional coplanar cracks represents areas of contact and non-contact explicitly. Deformations for a given pressure distribution and c/b ratio increased with increased crack spacing. For a given deformation, the contact area between the fracture faces was found to decrease with decreasing crack spacing. In order to match the observed deformation, calculations suggested that the contact area in the fracture zone was 60% or higher.

Further in-situ experiments on naturally occurring fractures are required, but results to date indicate that fracture stiffness, like other rock properties are a function of scale. This has important implications in extrapolating results of both hydrologic and seismic measurements at laboratory scales to field situations.

ACKNOWLEDGEMENTS

This work was supported through the U.S. Department of Energy Contract No. DE-AC03-76SF00098 by the DOE Office of Civilian Radioactive Waste Management, Office of Geologic Repositories. The work was done in cooperation with the Swiss National Cooperative for Nuclear Waste Storage (NAGRA). The authors are especially indebted to Stratis Vomvoris of NAGRA and Eric Wyss of Solexperts for their assistance in the field experiments. Special thanks are also due Professor Neville Cook and Professor George Cooper for their suggestions and invaluable assistance.

REFERENCES

Crouch, S. L. & Starfield, A. M. 1983. Boundary element methods in solid mechanics: with applications in rock mechanics and geological engineering. London, Boston: Allen & Unwin.

Hopkins, D. L., Cook, N. G. W. & Myer, L. R. 1987. Fracture stiffness and aperture as a function of applied stress an contact geometry. Proc. 28th U.S. Symp. Rock Mech., University of Arizona, Tucson, Arizona, June 29-July 1, 1987.

Myer, L. R., Pyrak-Nolte, L. J., Hopkins, D. L. & Cook, N. G. W. 1990. Seismic characterization of fracture properties. To be published First Annual International High Level Radioactive Waste Management Conference, American Nuclear Society.

Pyrak, L. J. 1988. Seismic visibility of fractures. Ph.D dissertation, University of California, Berkeley.

Pyrak-Nolte, L. J., Myer, L. R., Cook, N. G. W. 1990. Transmission of seismic waves across single fractures. Accepted for publication J. Geophys. Res.

Schoenberg, M. 1980. Elastic wave behavior across linear slip interfaces, J. Acoust. Soc. Am. Vol. 68, No. 5.

LAWRENCE BERKELEY LABORATORY
TECHNICAL INFORMATION DEPARTMENT
1 CYCLOTRON ROAD
BERKELEY, CALIFORNIA 94720